THE JOURNAL OF PHYSICAL CHEMISTRY C

Article

pubs.acs.org/JPCC

Interaction of Water with the CaO(001) Surface

Yuichi Fujimori,[†] Xunhua Zhao,[‡] Xiang Shao,[†,§] Sergey V. Levchenko,[‡] Niklas Nilius,[†,∥] Martin Sterrer,[*,†,⊥] and Hans-Joachim Freund[†]

[†]Department of Chemical Physics and [‡]Theory Department, Fritz-Haber-Institut der Max-Planck-Gesellschaft, Faradayweg 4-6, 14195 Berlin, Germany

[∥]Institute of Physics, Carl-von-Ossietzky University, 26111 Oldenburg, Germany

[⊥]Institute of Physics, University of Graz, Universitätsplatz 5, 8010 Graz, Austria

Supporting Information

ABSTRACT: The interaction of water with the CaO(001) surface has been studied from ultrahigh-vacuum to submillibar water vapor pressures and at temperatures of 100 and 300 K using well-structured CaO(001)/Mo(001) thin-film model systems. Infrared reflection absorption spectroscopy (IRAS), X-ray photoelectron spectroscopy (XPS), and scanning tunneling microscopy (STM) in combination with density functional theory (DFT) calculations have been employed to reveal the correlation between the vibrational frequencies of the hydroxyl groups and the distinct hydroxylated surface phases that develop as a function of water exposure. In the low-coverage regime, water monomers, small water clusters, and one-dimensional water chains are formed on the CaO(001) surface. At increasing water coverages, water-induced structural disorder is observed, indicating partial solvation of Ca^{2+} ions. Partial transformation of CaO(001) into a $Ca(OH)_2$-like phase occurs upon dosing of water at submillibar water pressure. In addition, it was found that interfacial hydroxyl groups formed on the CaO(001) surface during water exposure at temperatures as low as 100 K shift the temperatures for ice desorption and for the transition from amorphous solid water to crystalline ice by 10 K as compared to those for the nonhydroxylated MgO surface.

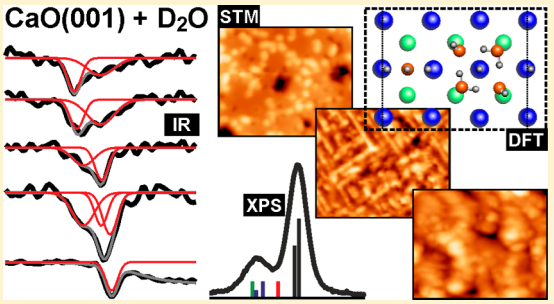

1. INTRODUCTION

The interaction of water with metal oxide surfaces is of interest because of the versatile roles of water in astrophysics, electrochemistry, geochemistry, solar energy production, and heterogeneous catalysis. Nevertheless, in contrast to water/metal interfaces,[1,2] atomic-scale information on water/oxide interfaces is limited, regardless of their abundance and rich chemical functionality. This deficiency is related to the inherent complexity of oxide surfaces: Their reactivity toward water depends on various parameters, such as the ionicity (covalency) of the metal−oxygen bond, the lattice constant, the defect structure, and the surface orientation.[3,4] Hence, an approach taking advantage of well-defined, simple model oxide surfaces is required to gain a fundamental understanding of the interaction. In this study, we use single-crystalline CaO thin films grown on a Mo(001) substrate to reveal the interaction of water with this surface from a fundamental point of view.

Among the binary metal oxides, the alkaline earth oxides are relatively simple in terms of their geometric and electronic structures. Of these, MgO has received most attention in fundamental research because structurally well-defined and stable surfaces of MgO in various forms (single crystals,[5−7] thin films,[8,9] nanoparticles[10,11]) can be prepared. In contrast, CaO and SrO have been less frequently investigated. This is partly due to the fact that their high reactivities toward gases, in particular, the environmentally omnipresent water and carbon dioxide, often impede the sustainability of well-structured and clean surfaces of these oxides, even under ultrahigh-vacuum (UHV) conditions. Conversely, this high reactivity forms the basis for many applications. For example, CaO is used in desulfurization processes,[12,13] in carbon capture (calcium looping),[14,15] and in heterogeneous catalysis as a basic catalyst or promoter.[16−19] The hydration and dehydration of CaO and the extent of hydroxylation/hydroxyl coverage are suggested to play essential roles in these processes.[17,20,21]

To date, only a few experimental studies have addressed the hydroxylation of CaO in a fundamental and systematic way. Low et al. investigated water (H_2O and D_2O) adsorption on CaO powder obtained from the thermal decomposition of $Ca(OH)_2$ using infrared spectroscopy.[22] Although several subsequent articles have reported infrared spectra of hydroxylated CaO as well, Low et al.'s investigation, which dates back to 1971, is the only study in which water coverage was varied in a systematic way. According to the results, Low et al. provided a basic model for the interaction of water with the CaO surface that evolves from water dissociation at low coverage to a partial transformation into a "pseudo"-brucite [$Ca(OH)_2$] structure at high exposure. Calorimetric measurements revealed that the

Received: January 14, 2016
Revised: February 16, 2016
Published: February 17, 2016

DOI: 10.1021/acs.jpcc.6b00433
J. Phys. Chem. C 2016, 120, 5565−5576

dissociative adsorption of water on CaO surfaces releases a greater amount of energy than the formation of $Ca(OH)_2$.[23] Through the use of synchrotron-based photoemission spectroscopy, Liu et al. found that the surface of a CaO(001) single crystal becomes hydroxylated even at vapor pressures below 5 × 10^{-9} Torr and that the bulk hydration of CaO toward $Ca(OH)_2$ occurs upon water exposure above 1 × 10^{-4} Torr.[24] This result was supported by a recent spectroscopic study using a thin CaO film grown on Si(100).[25] Iedema et al., using MgO(001) and CaO(001) thin films grown on a Mo(001) substrate, compared water adsorption on these two oxides with thermal desorption spectroscopy.[26] As expected from the different basicities of the two oxides, their analysis showed that monolayer water structures are thermally more stable on CaO than on MgO. Interestingly, the desorption of water ice from the oxides at temperatures below 200 K was also found to be different, and Iedema et al. speculated that this difference is related to the specific interfacial water structures and their interactions with the ice layers.[26]

The above-mentioned surface-science-oriented single-crystal and thin-film studies suffered in general from poorly characterized sample surfaces. Recently, the Fritz-Haber-Institut (FHI) group succeeded in growing well-defined CaO(001) films on a Mo(001) substrate and characterized them by low-energy electron diffraction (LEED) and scanning tunneling microscopy (STM).[27] In addition, substitutional Mo ions that entered the rock-salt lattice through either diffusion from the Mo support or intentional doping were found to alter the binding properties of admetals and molecules.[28,29] Recently, some of us showed that one-dimensional water adstructures are stabilized on thick, bulk-like CaO(001)/Mo(001) films under certain conditions.[30]

Herein, we report the interaction of water (D_2O) with the surface of CaO(001) thin films grown on a Mo(001) substrate over wide pressure and temperature ranges as studied by means of X-ray photoelectron spectroscopy (XPS) and infrared reflection absorption spectroscopy (IRAS) in combination with STM and density functional theory (DFT) calculations. The main goals of this work were the exploration of surface hydroxylation under UHV and elevated-pressure conditions (0.05 mbar) and substrate temperatures of 100−300 K, as well as the thermal behavior of amorphous solid water (ASW) condensed on the CaO(001) surface. We demonstrate that different hydroxyl structures can be obtained under different water-dosing conditions and address the correlation between surface hydroxyl groups and the thermal behavior of ASW, including its phase transition to crystalline ice (CI).

2. EXPERIMENTAL AND COMPUTATIONAL METHODS

2.1. Experimental Methods. The experiments were performed in a UHV chamber equipped with LEED optics and a hemispherical electron energy analyzer (Specs, Phoibos 150). The base pressure of the chamber was maintained at 2 × 10^{-10} mbar. IR data were collected in a stainless steel UHV/high-pressure cell attached to the main UHV chamber using a Bruker IFS66v/S spectrometer and a mercury cadmium telluride (MCT) detector. The Mo(001) sample was cleaned by Ar^+ sputtering (10^{-5} mbar, 1.5 keV), annealing to 1300 K in an oxygen atmosphere of 1.0 × 10^{-7} mbar, and subsequent flashing to 2300 K by electron bombardment, as measured with a pyrometer. This procedure was repeated until a sharp Mo(001)-(1 × 1) LEED pattern was obtained and no contamination (in particular, no carbon segregation from the bulk) was observed by XPS. Afterward, a type-K thermocouple was spot-welded to the sample for better temperature control. Because of the limited thermal stability of the type-K thermocouple, subsequent cleaning of the Mo(001) substrate was performed by repeated cycles of Ar^+ sputtering and annealing to 1200 K. The CaO(001) film was grown onto the Mo(001) surface by depositing Ca (99.9%, Goodfellow) at an oxygen background pressure of 1 × 10^{-7} mbar and a substrate temperature of 300 K by physical vapor deposition (Omicron, EFM3T). The as-grown CaO film was annealed to 1200 K in vacuo for 10 min, resulting in a highly crystalline CaO(001) surface (Figure 1).[27] Careful removal of water residuals from

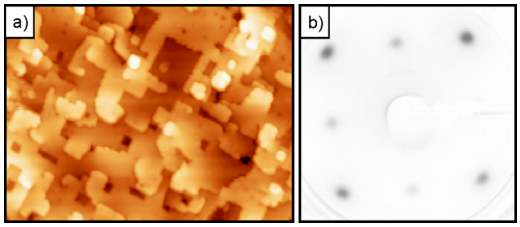

Figure 1. Structure and morphology of CaO(001) films used in this study: (a) STM topographic image of the oxide layer prior to water adsorption (100 × 70 nm^2, 3.5 V). (b) LEED pattern of the 25-ML-thick film (electron energy = 100 eV).

the chamber, the Ca evaporant, and the oxygen gas was essential for the preparation of clean and well-structured CaO(001) films. Films thicker than 10 ML were prepared by sequential CaO depositions onto a thin CaO(001) template surface with good quality. D_2O (99.75%, Merck) was purified by repeated freeze−pump−thaw cycles and exposed to the CaO films at a substrate temperature of 300 or 100 K in the UHV/high-pressure cell. D_2O doses are given in units of Langmuir (L), with 1 L = 1 × 10^{-6} Torr·s. Minor contamination of the CaO(001) surface during exposure at elevated water partial pressure (millibar range) could not be avoided. XPS and IR signals typical of carbonates (C 1s peak at a binding energy of 291 eV and IR frequencies in the range 1200−1600 cm^{-1}) were detected after exposure to 0.05 mbar of D_2O. Based on a comparison of the hydroxyl O 1s and carbonate C 1s peak areas and taking into account the relative sensitivity factors for these core-level emissions, the concentration ratio of surface carbonate to surface hydroxyl was estimated to be <0.03. This small contribution is not expected to have any influence on our interpretation of the hydroxylation behavior of CaO at elevated pressure.

XP spectra were recorded with nonmonochromatized Al Kα radiation at an electron takeoff angle of 60° with respect to the surface normal. IR measurements were performed in reflection absorption mode. The resolution was set to 4 cm^{-1}, and 1000 scans were added for one spectrum. The spectrum of a freshly prepared and annealed CaO(001) surface was used for background correction for the adsorbate-covered surfaces. XPS and IRAS experiments were performed independent of each other to ensure that our interpretation of the IRAS results did not erroneously include any contribution of X-ray-induced water dissociation, if present. The STM experiments were performed in a different UHV chamber. Cleaning of the substrate and CaO film preparation were identical to the above procedures.

2.2. Theoretical Calculations. The theoretical calculations are performed with the FHI-aims electronic-structure program

DOI: 10.1021/acs.jpcc.6b00433
J. Phys. Chem. C 2016, 120, 5565−5576

package.[31] The Perdew–Burke–Ernzerhof (PBE)[32] and hybrid Heyd–Scuseria–Ernzerhof (HSE06)[33,34] exchange-correlation functionals, along with default-*tight* basis, were used to conduct periodic DFT calculations. A four-layer (3 × 4) slab was used to model the CaO(001) surface,[30] whereas a nine-layer (3 × 3) slab was used for the $Ca(OH)_2$ surface (see Supporting Information). The atomic relaxation and vibrational frequencies were calculated with the PBE functional. Two bottom CaO layers and six bottom $Ca(OH)_2$ layers were kept fixed during relaxation. The adsorption energies E_{ads} per water molecule were calculated with the HSE06 functional as follows

$$E_{ads} = \frac{1}{n}(E_{slab} + nE_{H_2O} - E_{nH_2O/slab}) + \Delta E^{ZPE}$$

where n is the number of water molecules per unit cell and $E_{nH_2O/slab}$, E_{slab}, and E_{H_2O} are the DFT total energies of the metal oxide slab with adsorbed water, the slab without water, and water molecules in the gas phase, respectively. The zero-point energy ΔE^{ZPE} was calculated as

$$\Delta E^{ZPE} = \frac{1}{n}(E^{ZPE}_{slab} + nE^{ZPE}_{H_2O} - E^{ZPE}_{nH_2O/slab})$$

where $E^{ZPE}_{nH_2O/slab}$, E^{ZPE}_{slab}, and $E^{ZPE}_{H_2O}$ are the corresponding zero-point energies (ZPEs).

In vibrational calculations, only the adsorbates and the surface oxygen atoms bonded to the adsorbates are allowed to move. Allowing surface Ca atoms and more O atoms to move changes the vibrational frequencies by at most 1–3 cm^{-1}. The calculated IR spectra were obtained using a finite-difference approach and the harmonic approximation.[35] The surface core-level shifts (SCLSs) were calculated based on the Slater–Janak transition-state approach[36,37]

$$\Delta_{SCLS} = \varepsilon_i^{KS}\left(\frac{1}{2}\right) - \varepsilon_{bulk}^{KS}\left(\frac{1}{2}\right)$$

where $\varepsilon_i^{KS}\left(\frac{1}{2}\right)$ and $\varepsilon_{bulk}^{KS}\left(\frac{1}{2}\right)$ are the Kohn–Sham eigenstate energies evaluated by self-consistent DFT calculations with the O 1s (Ca 2p) orbital half-occupied for surface and bulk O (Ca) species, respectively. These KS energies represent the calculated binding energies including the core-hole relaxation (i.e., final-state effects), and the difference between the KS core-level energies at full occupation correspond to the initial-state approximation. The compensating one-half electron was placed at the conduction-band minimum of the slab. All SCLSs were corrected for the vacuum-level shift for each system. As the bulk reference value, we used $\varepsilon_{1s}^{KS}\left(\frac{1}{2}\right)$ for the subsurface O or Ca in the perfect slab. All SCLS values were calculated with HSE06. For comparison, PBE SCLS values are reported in the Supporting Information. The difference between HSE06 and PBE SCLSs is in the range from −0.3 to 0.5 eV, depending on the adsorbate coverage and the position of the atom. We note that there can be an artificial shift in SCLSs because of the finite size of the supercells. To estimate this effect, we performed PBE SCLS calculations for selected systems using thicker slabs and longer lateral lattice vectors. We also used a simple electrostatic model (assuming the compensating charge to be uniformly distributed within the slab) to estimate the infinitely dilute limit. The periodic boundary conditions were found to affect the SCLS by at most ±0.2 eV.

3. RESULTS AND DISCUSSION

3.1. Hydroxylation and Hydration of CaO(001) Films.

The hydroxylation of bulk-like 25-ML CaO(001)/Mo(001) samples by exposure to water vapor was studied for three different water-dosing conditions: (1) by exposing water vapor at room temperature under UHV conditions [2-L dose at $p(D_2O) = 5 \times 10^{-9}$ mbar], (2) by condensing water onto the CaO surface at 100 K [5-L dose at $p(D_2O) = 5 \times 10^{-9}$ mbar] followed by heating to room temperature, and (3) by exposure to 0.05 mbar of D_2O at room temperature for 180 s.

The O 1s and Ca 2p XP spectra of the water-exposed samples, together with those of the clean CaO(001) surface, are compiled in panels a and b, respectively, of Figure 2. In addition

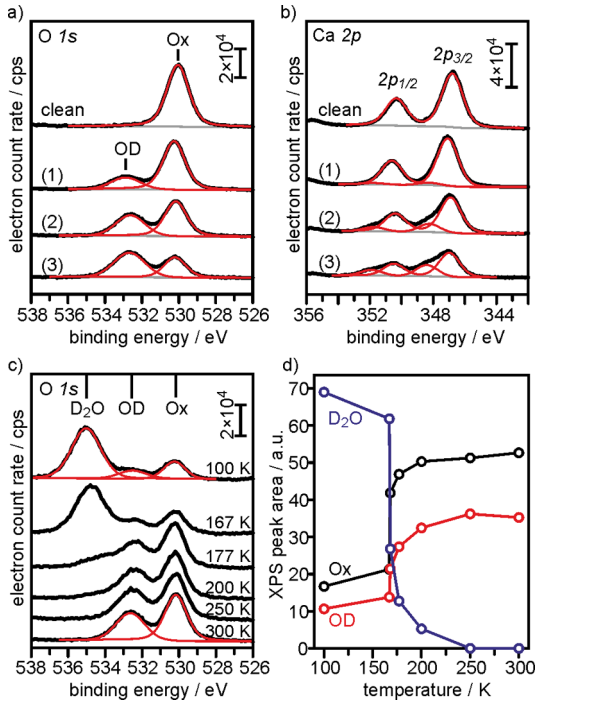

Figure 2. (a) O 1s and (b) Ca 2p XP spectra of 25-ML CaO(001) films and CaO(001) surfaces hydroxylated according to the following procedures: (1) exposure to 2 L of D_2O at room temperature, (2) exposure to 5 L of D_2O at 100 K and subsequent annealing to 300 K, and (3) exposure to 0.05 mbar of D_2O for 180 s at room temperature. (c) O 1s XP spectra acquired from CaO(001) films after application of procedure 2. Each data set was recorded at the indicated temperature. (d) Temperature dependence of the O 1s peak intensities ascribed to water (D_2O, blue trace), oxide ions (Ox, black trace), and hydroxyl groups (OD, red trace) for CaO(001) films hydroxylated by procedure 2.

to the oxide O 1s emission at a binding energy (BE) of 530.2 eV, the water-exposed films exhibit an O 1s component at 532.9 eV BE, which is assigned to hydroxyls. In accordance with previous surface-science investigations on CaO(001) single crystals and CaO films,[24,25] hydroxylation of CaO(001) was found to be highly effective under UHV conditions, as indicated by the presence of a clear hydroxyl O 1s peak already after a 2-L dose at room temperature (spectrum 1 in Figure 2a). The simultaneous intensity decrease of the main O 1s component indicates the partial transformation of lattice O^{2-} ions into OH^- species.

A substantial enhancement of the hydroxyl coverage was obtained by water dosing following procedure 2. Exposure at

DOI: 10.1021/acs.jpcc.6b00433
J. Phys. Chem. C 2016, 120, 5565–5576

submillibar water pressures (procedure 3) further increases the hydroxyl coverage and causes the hydroxyl/oxide O 1s peak ratio to shift toward the hydroxyl component (Figure 2a). The simultaneous appearance of a high-BE shoulder in the Ca 2p region at 348.4 eV BE (Ca $2p_{3/2}$), which is shifted by +1.4 eV compared to the main Ca 2p line of CaO(001),[24] confirms the hydroxylation of the CaO surface (Figure 2b). The observed core-level BE shift is in good agreement with the difference in the calculated Ca 2p core-level BEs of CaO and $Ca(OD)_2$, which we found to be roughly 1.0−1.5 eV (see Table S2, Supporting Information). Our analysis of the Ca 2p core-level shift between CaO(001) and $Ca(OD)_2$ shows that it is entirely due to different final-state screening effects, as the difference in the initial states is only 0.06 eV (see Table S3, Supporting Information).

The hydroxyl coverage was calculated following the procedure reported in ref 24. Using the OD/oxide XPS peak intensity ratio determined by peak fitting and the electron mean free path for the O 1s kinetic energy under Al Kα excitation, we obtained half- and full monolayer hydroxyl coverage after water dosing according to procedures 1 and 2, respectively. For dosing at submillibar water pressure, a hydroxyl coverage above 1 ML is revealed, which indicates that hydroxylation extends partially into the bulk under these conditions.[24]

Figure 2c presents a series of O 1s XP spectra recorded during heating of the water layers condensed at 100 K onto a clean, unhydroxylated CaO(001) surface. Three components are clearly discernible in the 100 K spectrum. The one at highest BE (535.3 eV) can be attributed to the O 1s emission of molecular water in water ice, the middle one is related to the hydroxyls, and the low-BE contribution corresponds to the substrate O 1s peaks. Note that the substrate and interface signals are strongly attenuated because of the presence of the ice layer. The experiment thus shows that water dissociates on the CaO(001) surface already below 100 K, which is in line with previous DFT calculations.[38] Heating to 166 K causes no significant changes. After heating to 177 K, however, the peak for molecular water disappears, and the substrate- and interface-related signals gain intensity, indicating desorption of large parts of the ice layer. Water ice is completely gone after heating to 200 K, leaving the hydroxylated CaO(001) surface exposed. The spectra remain unchanged upon further heating to 300 K. The temperature-dependent intensities of the ice, hydroxyl, and oxide O 1s peaks, obtained from corresponding fitting procedures, are shown in Figure 2d. Most notably, the peak intensity ratio of the oxide and hydroxyl contributions does not change significantly between 100 and 300 K, suggesting that almost no additional water dissociation occurs during this heating step.

The IRA spectra associated with the hydroxylation states represented by the XP spectra in Figure 2a are shown in Figure 3a. In accordance with the XPS data, the intensity of hydroxyl-(OD-) related IR signals increases from procedure 1 to procedure 3, that is, with increasing hydroxyl coverage. IR spectra of strongly hydroxylated (OD) oxide surfaces, in general, can be divided into the regions above and below 2700 cm^{-1} (3700 cm^{-1} for OH).[39] Above 2700 cm^{-1}, typically narrow IR signals due to the stretching vibrations of free (non-hydrogen-bonded) and hydrogen-bond-acceptor hydroxyls are found. On the lower-frequency side are the vibrations of multicoordinated, hydrogen-bond-donor hydroxyls and those of molecularly adsorbed water. In the present study, the latter domain exhibits only broad vibrational contributions peaking at

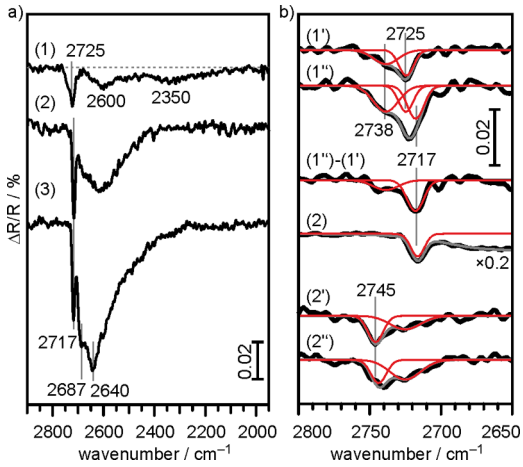

Figure 3. (a) IRA spectra of hydroxylated CaO(001) films prepared according to procedures 1−3. All spectra were acquired at a sample temperature of 300 K. (b) IRA spectra of CaO(001) films after exposure to (1′) 0.15 and (1″) 2.0 L of D_2O in total at room temperature. The spectrum labeled 1″ − 1′ is the result of spectral subtraction of the corresponding spectra. IRA spectrum 2 corresponds to procedure 2 with subsequent annealing to 300 K, whereas IRA spectra 2′ and 2″ were acquired after exposure to a total of 0.15 and 0.3 L of D_2O, respectively, at 100 K.

2600 cm^{-1} after the application of procedures 1 and 2. In addition, a rather broad absorption maximum extending from 2500 to 2000 cm^{-1} is observed for dosing procedure 1. On top of the broad 2600 cm^{-1} band, the CaO(001) sample exposed to submillibar water pressures (procedure 3) exhibits two rather narrow OD signals at 2687 and 2640 cm^{-1}, with the former being close to the characteristic OD stretch vibration in pure $Ca(OD)_2$ observed at 2689 cm^{-1}.[40] In the high-frequency domain (>2700 cm^{-1}), a band at 2725 cm^{-1} with a high-frequency shoulder is present on the low-dose, room-temperature-exposed sample (procedure 1), whereas hydroxylation procedures 2 and 3 yield a single band at 2717 cm^{-1}.

In Figure 3b, detailed IR spectra near 2700 cm^{-1} are presented for various dosing conditions and water coverages. Spectra 1′ and 1″ are IRA spectra collected after exposure of CaO(001) to 0.15 and 2 L of D_2O, respectively, at room temperature. Spectral fitting reveals the presence of at least two vibrations at 2725 and 2738 cm^{-1} in the low-coverage regime (spectrum 1′). The spectrum corresponding to saturation coverage of water at room temperature (spectrum 1″, 2 L of D_2O) exhibits, apart from an overall increased absorption intensity, almost the same spectral profile. However, spectral subtraction (1″ − 1′) reveals the development of a new band at 2717 cm^{-1}, as well as a further increase of the component at 2738 cm^{-1} at higher coverage. The OD peak at 2717 cm^{-1} that is exclusively formed on high-coverage samples (spectra 2 and 3 in Figure 3a and spectrum 2 in Figure 3b) is assigned to vibrations of closely spaced surface hydroxyls (OD) or hydroxyls interacting with molecularly adsorbed water on fully hydroxylated CaO surfaces. The observation of OD vibrations at 2738 and 2725 cm^{-1} on the partially hydroxylated films hints at the presence of various water adsorption structures on this surface.

With the aim of obtaining more information about molecular or dissociatively adsorbed isolated water molecules or small water aggregates on the CaO(001) surface, IRA spectra were acquired after the dosing of small quantities of water at 100 K.

DOI: 10.1021/acs.jpcc.6b00433
J. Phys. Chem. C 2016, 120, 5565−5576

An initial dose of 0.15 L of D_2O (spectrum 2′ in Figure 3b) leads to the development of a narrow band at 2745 cm^{-1}, accompanied by small and broad contributions at the low-frequency side of the signal. The latter signal gains intensity upon further dosing of 0.15 L of D_2O (0.3 L in total, spectrum 2″ in Figure 3b; an additional small and broad signal at 2630 cm^{-1} appears at this dose), whereas the narrow band at 2745 cm^{-1} has apparently saturated already after the first dose. This high-frequency band is therefore attributed to water monomers, whereas the lower-frequency contributions are likely due to water/hydroxyl clusters.

3.2. Thermal Stability of Hydroxyls on CaO(001) Films. In addition, XPS and IRAS were applied to follow the dehydroxylation of the hydroxylated CaO(001) surfaces. A summary of the XPS results is shown in Figure 4a, which displays the absolute hydroxyl O 1s photoemission peak areas obtained for the three preparation procedures 1−3, as well as the corresponding calculated OD coverage in monolayers as a function of annealing temperature. Note that absolute OD coverages cannot be given for samples prepared according to procedure 3, because of partial bulk hydroxylation in this case.

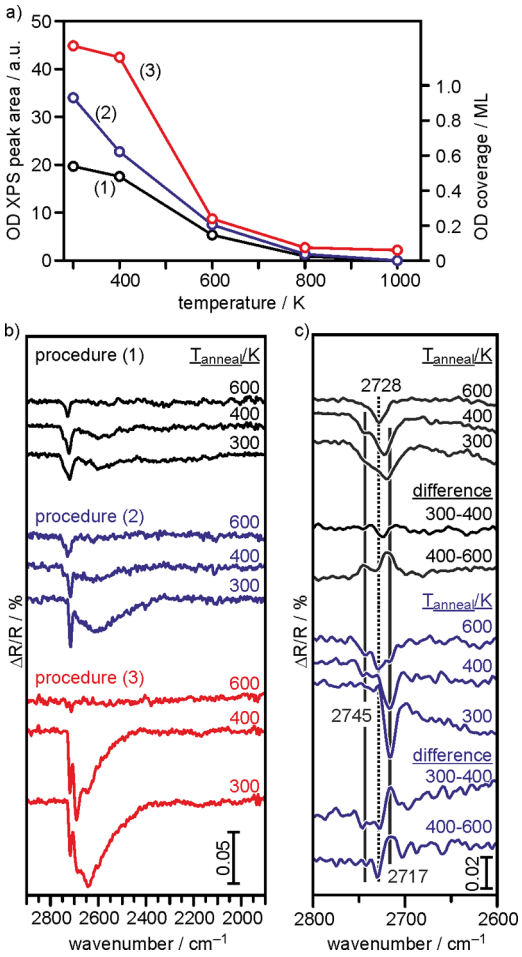

Figure 4. (a) Hydroxyl O 1s peak intensities (and corresponding hydroxyl coverages) of hydroxylated CaO as a function of annealing temperature. The various curves show the results for different initial hydroxyl coverages (according to hydroxylation procedures 1−3). (b) Corresponding IRA spectra. (c) Details of the IR spectra from panel b near 2700 cm^{-1} for procedures 1 (black) and 2 (blue), together with the results of spectral subtraction.

Strong dehydroxylation of CaO occurs upon heating to 600 K, where the hydroxyl coverage drops to 0.2 ML for all samples, independent of the hydroxylation history. A clean, hydroxyl-free CaO(001) surface is restored after further heating to 1000 K.

At lower temperatures, hydroxylation states resulting from preparation procedures 1 and 3 are relatively stable up to 400 K, whereas the OD coverage drops from 1 to 0.6 ML upon heating to 400 K after application of dosing procedure 2. This trend is also reflected by the IRAS results shown in Figure 4b, where we plot for each hydroxylation procedure the spectra acquired after room-temperature hydroxylation and after heating to 400 and 600 K (from bottom to top). In agreement with the XPS results, the 300 and 400 K IRA spectra from hydroxylation procedure 1 are almost identical. For procedure 2, however, the IRA spectrum changes significantly upon heating to 400 K, reaching a state where the intensity is similar to that for procedure 1 at 400 K. Upon heating to 600 K, the spectra simplify, and a single band at ν(OD) = 2728 cm^{-1} remains. A more detailed view of the region near 2700 cm^{-1} is shown in Figure 4c, where, in addition to the spectra acquired after various annealing steps, the corresponding difference spectra are displayed. As noted above, heating to 400 K causes only minor changes in the spectra of the CaO films hydroxylated by procedure 1 (black curves). The intensity of the bands remains almost unchanged, and only small shifts in the band maxima are noted, indicative of slight rearrangements in the hydroxyl layer. The difference spectrum (300 − 400 K) reveals the appearance of a signal at 2725 cm^{-1} (negative signal in the spectrum) at the expense of low- and high-frequency contributions. Partial dehydroxylation upon heating to 600 K results in an almost complete loss of the low- and high-frequency OD signals at 2717 and 2745 cm^{-1}, whereas the band at 2728 cm^{-1} remains. This trend in stability is consistent with observations made during the adsorption of water at room temperature (Figure 3b), where the 2717 and ∼2740−2745 cm^{-1} bands appeared at increasing water coverages, indicating weaker binding of the underlying adsorbate structures.

For hydroxylated CaO prepared by procedure 2 (Figure 4c, blue), weakly bound water is removed during heating to 400 K. This involves loss of absorption intensity of the broad OD feature at about 2600 cm^{-1} but also of the narrow 2717 cm^{-1} band. At the same time, signals in the frequency range of 2720−2745 cm^{-1} appear. This trend continues upon heating to 600 K, with almost complete loss of the 2717 cm^{-1} signal and appearance of a band at 2728 cm^{-1}. For the strongly hydroxylated sample (procedure 3, red spectrum in Figure 4b), dehydroxylation follows a trend similar to that previously reported for CaO powder:[22] The loss of the broad contribution at about 2640 cm^{-1} during heating to 400 K is accompanied by a slight intensity increase of the narrow bands at 2687 and 2717 cm^{-1}.

3.3. Adsorption Structures, Calculated IR Spectra, and Interpretation of IR Results. Before analyzing the results of the present study, we summarize some findings of previous works related to the hydroxylation of CaO. To date, only a few experimental studies have aimed at a fundamental understanding of the hydroxylation of the CaO(001) surface. The one closest to the present work was an infrared study by Low et al.,[22] the main results of which are reproduced in Figure 5.

In that work, $Ca(OH)_2$ powder was initially activated at a temperature of 973 K. The presence of a sharp OH (OD) signal at 3695 (2719) cm^{-1} after thermal activation points to incomplete dehydroxylation or fast rehydroxylation of the CaO

DOI: 10.1021/acs.jpcc.6b00433
J. Phys. Chem. C 2016, 120, 5565−5576

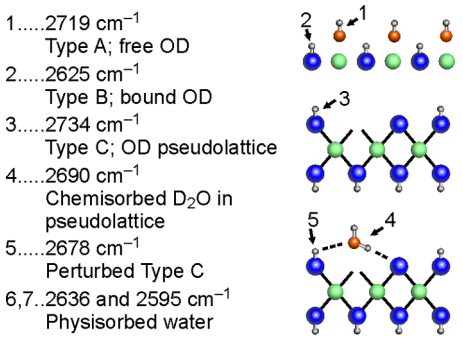

Figure 5. OD frequencies and band assignments for hydroxylated CaO according to Low et al.[22] The corresponding structural models, except for physisorbed water, are shown in the right panel. Blue, O atom of CaO; green, Ca atom of CaO; orange, O atom of water adspecies; gray, hydrogen (deuterium) atom.

surface in this experiment. After dosing of water onto the surface, several new OH (OD) species formed. Signals 1 and 2 (type A and B hydroxyls) were thus assigned to "regular" singly and multiply coordinated hydroxyls on the CaO surface (Figure 5, right panel, top), whereas signals 3–5, which developed only after the largest water doses, were attributed to $Ca(OH)_2$-like hydroxyls and strongly bound water (Figure 5, right panel, bottom). Note that pure $Ca(OH)_2$ lacks any hydrogen-bond interaction between the hydroxyl groups and gives rise to a single sharp OH stretch signal at 3645 cm^{-1} [or 2689 cm^{-1} for $Ca(OD)_2$].[40] Low et al.[22] concluded from their study that a substantial degree of hydrogen-bond interaction between the hydroxyls remains even at the highest water doses, indicating an incomplete transformation of CaO into $Ca(OH)_2$ [$Ca(OD)_2$]. Therefore, they attributed signals 4 (chemisorbed water) and 5 (type C hydroxyls) to vibrations originating from a $Ca(OH)_2$ pseudolattice. This pseudolattice was assumed to be a distorted and imperfect brucite structure with vacancy defects or oxide anions in hydroxyl positions (Figure 5, right panel, middle) that facilitates hydrogen-bond interactions between neighboring hydroxyls. In addition, they noted that unperturbed type C hydroxyls of the pseudolattice (3703 cm^{-1} for OH, 2734 cm^{-1} for OD; signal 3) are also present after mild thermal activation of $Ca(OH)_2$.

Table 1 summarizes relevant IR frequencies observed on CaO thin films in this study. According to the quantitative XPS analysis presented above, the hydroxylation of the CaO surface leads to two different states: Surface-only hydroxylation occurs for all hydroxylation treatments performed in the low-pressure regime (procedures 1 and 2, Figure 2), whereas surface plus partial bulk hydroxylation is observed at near-ambient water vapor pressure (procedure 3, Figure 2). Depending on the surface hydroxylation state, the IR spectra reveal some characteristic features: For small doses of water at a sample temperature of 100 K, an OD band with $\nu(OD)$ = 2745 cm^{-1} is observed that is not accompanied by an additional OD contribution at lower frequency (Figure 3b). In the experiments reported here, this band reaches saturation already after the first water dose, and subsequent water exposure at 100 K leads to the formation of an additional hydroxyl band with $\nu(OD)$ = 2725 cm^{-1} and contributions at 2600 cm^{-1}. It is noted that water dosing at 300 K results in the formation of hydroxyl groups with the same vibrational frequencies, but slightly different abundances (Figure 3b).

The hydroxylated CaO surface prepared by adsorption of water at low temperature (100 K) followed by annealing to 300 K (procedure 2), yielding an OD coverage of 1 ML, exhibits a single sharp OD band at 2717 cm^{-1}, accompanied by a broad and featureless signal centered at about 2600 cm^{-1} (Figure 3a). For the CaO surface exposed to 0.05 mbar of D_2O, where hydroxylation extends partially into the bulk of the material, the IRAS data show, in addition to the broad contribution at 2600 cm^{-1}, three distinct signals at 2717, 2687, and 2643 cm^{-1} (Figure 3a).

In Table 1, the signals observed for hydroxylated CaO thin films having frequencies similar to those detected for CaO powders are labeled according to the numbering given in ref 22. In particular, for the strongly hydrated state (exposure to 0.05 mbar of D_2O at room temperature), the two results match well, suggesting that similar hydrated states are obtained on extended surfaces and powders after hydroxylation at near-ambient conditions. However, for the weakly hydrated state, our spectra contain more information, mainly because the UHV-based preparation scheme keeps the CaO films clean and hydroxyl-free before the start of the actual IR experiments. In fact, the initial IR spectrum in ref 22 probes the CaO powder already in a hydroxylated state, because the primary band at $\nu(OD)$ =

Table 1. Summary of OD-IRAS Signals on CaO(001) Observed in This Study for Various D_2O Doses[a] and Hydroxyl Coverages[b,c]

Band No.	1a	1b	3	1c	1	5	6	2,7	OD coverage
OD / cm^{-1}	2745	2738	2728	2725	2717	2687	2643	2600(b)	
0.15 L D_2O, 100 K (2)	●	◖							< 0.2 ML
0.3 L D_2O, 100 K (2)	●	●		◖				●	< 0.5 ML
0.15 L D_2O, 300 K (1)		◖		●					< 0.2 ML
0.15-2L D_2O, 300 K (1)		●		●	◖			●	max 0.5 ML
1 L D_2O, 100 K → 300 K (2)					●			●	1 ML
0.05 mbar D_2O, 300 K (3)					●	●	●	●	> 1 ML
Anneal 600 K (1),(2),(3)			●						< 0.5 ML

[a]Hydroxylation procedures indicated in parentheses. [b]Signals are labeled according to the numbering given in Figure 5,[22] and assignments are discussed in the text. [c]Solid circle and half-circle symbols indicate the relative intensity/abundance of the signals in the spectra.

DOI: 10.1021/acs.jpcc.6b00433
J. Phys. Chem. C 2016, 120, 5565−5576

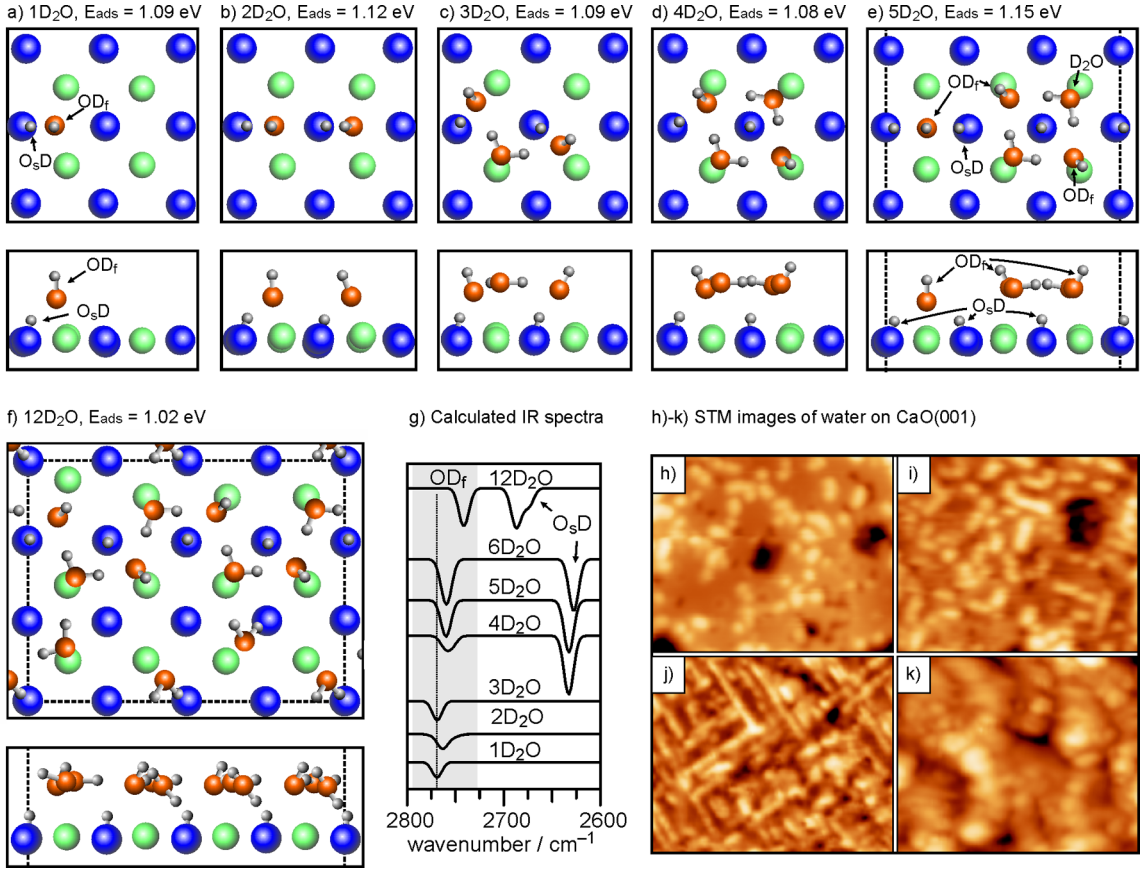

Figure 6. Structural models of (a) single OD−D pair ($1D_2O$), (b) water dimer ($2D_2O$), (c) water trimer ($3D_2O$), (d) water tetramer ($4D_2O$), (e) water pentamer ($5D_2O$), and (f) water dodecamer ($12D_2O$), as obtained from a first-principles genetic algorithm.[30] [A (3 × 4) CaO(001) unit cell was used in the calculations.] The free OD groups (OD_f) and surface OD groups (O_sD) are indicated in the $1D_2O$ and $5D_2O$ structures. Blue, O atom of CaO; green, Ca atom of CaO; orange, O atom of water adspecies; gray, hydrogen (deuterium) atom. (g) Calculated (harmonic approximation) IR spectra of submonolayer water structures on CaO containing 1−6 and 12 water molecules in a (3 × 4) unit cell. Only the 2600−2800 cm^{-1} spectral region is shown, and the signals of OD_f are highlighted. The spectra are broadened by Gaussians of 10 cm^{-1} fwhm. (h−k) STM topographic images (30 × 25 nm^2) of 10-ML-thick CaO(001) films exposed to water: (h) 0.05 L of D_2O dosed at 77 K, (i) 0.1 L of D_2O dosed at room temperature, (j) 0.3 L of D_2O dosed at room temperature, and (k) saturation dose of D_2O at room temperature.

2717 cm^{-1} (band 1) emerges in our UHV study only at monolayer OD coverage. The bands labeled as 1a, 1b, and 1c (2745, 2738, and 2725 cm^{-1}, respectively) in Table 1 can, therefore, be assigned to adsorbed hydroxyls in adstructures corresponding to submonolayer coverage.

For water monomer adsorption, DFT predicts the minimum-energy structure to be a tight D−OD ion pair (Figure 6a), with the OD group adsorbed in a bridge position between two Ca^{2+} ions ("free OD", OD_f), and the proton being transferred to the next nearest oxygen ion ("surface OD", O_sD).[38] Molecular dynamics simulations suggest that the proton is pinned as the OD group revolves around the proton.[38] In the low-coverage regime, a recent experimental and computational study found one-dimensional water/hydroxyl chains on the surface of CaO(001) to be stable at room temperature.[30] The most stable adsorption structures for the water dimer ($2D_2O$), trimer ($3D_2O$), tetramer ($4D_2O$), and pentamer ($5D_2O$) found by a genetic algorithm search are shown in Figure 6b−e.[30]

Isolated water/hydroxyl clusters are formed up to the tetramer, whereas the pentamer represents the first water/hydroxyl chain structure, which consists of tetramer units linked by a dissociated water molecule. The hexamer ($6D_2O$, not shown) forms a chain structure similar to that found for $5D_2O$, with the difference that the fifth and sixth water molecules form linkers at opposite sides of the tetramer unit. Note that the one-dimensional chain structures ($5D_2O$ and $6D_2O$) are the most stable configurations among the investigated structures (compare the adsorption energies, E_{ads}, per D_2O molecule noted in Figure 6).[30] In contrast to water adsorbed on MgO, two-dimensional water/hydroxyl structures (e.g., $12D_2O$, Figure 6f) are less stable than the one-dimensional structures and the smaller clusters on CaO(001).[30] Calculated harmonic spectra of the dissociated water monomer ($1D_2O$) and other adsorption structures emerging with increasing coverage, including the $5D_2O$ structure, are shown in Figure 6g. [See Table S1 in the Supporting Information for the corresponding sets of calculated harmonic vibrational frequencies for water adsorption structures containing 1−6 and 12 water molecules per (3 × 4) CaO unit cell.] To facilitate comparison with the experimental spectra, only the component of the dipole moment perpendicular to the surface has been evaluated, because the metal surface selection rule, which also applies for thin-film samples, restricts observation to these vibrational components. The high-frequency bands in the calculated spectra correspond to the OD_f groups. In general, they exhibit the highest frequency in the low-coverage structures ($1D_2O$) and shift to lower frequency as the coverage is increased, that is, with increasing hydrogen-bond interactions (two-dimensional

DOI: 10.1021/acs.jpcc.6b00433
J. Phys. Chem. C 2016, 120, 5565−5576

network in $12D_2O$). The nonmonotonic trend seen in the calculated spectra for the intermediate coverages results from the presence of OD_f groups in distinct environments: The OD_f frequencies are equivalent in $1D_2O$ and $3D_2O$ because the corresponding OD_f groups are coordinated to one surface hydroxyl, O_sD, in both structures. This interaction is only weakly perturbed by the additional molecular water in the case of $3D_2O$. In $2D_2O$, where both water molecules are dissociated, one of the OD_f groups is coordinated to two O_sD groups, leading to a red shift as a result of the increased hydrogen-bond interaction. This structural feature is also found in the linker element between tetramer units in the water chains originating from $5D_2O$ and $6D_2O$. Its frequency is similar to those of the OD_f groups of the tetramer units, and as such, the OD_f bands of $2D_2O$, $4D_2O$, $5D_2O$, and $6D_2O$ appear at roughly the same spectral position (Figure 6g).

For O_sD, one can also distinguish two cases: those associated with OD_f groups in close proximity, which are present in the small water clusters ($1D_2O$-$4D_2O$) and in the linker units of the chain structures ($5D_2O$ and $6D_2O$), and those contained in the center of the tetramer units in $4D_2O$−$6D_2O$, which are surrounded by two undissociated water molecules and two OD_f groups (Figure 6d,e). Note that the former are tilted and exhibit strongly elongated O−D bonds. Correspondingly, their vibrations are found at low frequencies (in the range of 1800−2300 cm^{-1}, Table S1). For O_sD groups inside the tetramer units, the interaction with OD_f is partly screened by the in-plane hydrogen-bond interaction between OD_f groups and molecular water. These less perturbed O_sD groups thus exhibit higher vibrational frequencies (bands at 2630 cm^{-1} in Figure 6c). For the two-dimensional network represented by the $12D_2O$ structure (Figure 6f), the spectral separation of the OD_f and O_sD contributions decreases further because of the larger degree of in-plane hydrogen bonding, which weakens the O−D bond in OD_f groups and leads to a further red shift. Conversely, the O_sD groups are less engaged in hydrogen-bond interactions, leading to a blue shift of their stretching frequency (Figure 6g).

In addition to the theoretical results presented above, we include STM images of CaO(001) films taken as a function of water exposure to examine structural and morphological changes induced by water adsorption. After the dosing of small amounts of water at 77 K, individual round protrusions and larger aggregates of these protrusions appear on the surface (Figure 6h). Consistent with the dose, each protrusion can be identified as a single undissociated or dissociated water molecule, and the aggregates correspond to small water/hydroxyl clusters. At room temperature and water coverages up to 0.3 ML, linear water/hydroxyl chains oriented along the CaO[110] directions are the most stable adsorption structures (Figure 6i,j).[30] When the water coverage is increased above this limit, disordered water-induced adlayers are observed (Figure 6k). With this additional STM and theoretical input, the IRAS observations in the submonolayer/UHV regime can be interpreted as follows:

The sharp band at 2745 cm^{-1} observed at low water exposure at 100 K (Figure 3b) is attributed to the OD_f vibration of the tight ion pair proposed by the DFT calculations.[38] The growing contributions at the low-frequency side of this band at higher dose then correspond to the OD vibrations of larger water/hydroxyl aggregates (dimers, tetramers). This interpretation is consistent with the calculated IR spectra of these entities, which feature free OD (OD_f) groups with stretching frequencies slightly red-shifted compared to those of the dissociated monomer (Figure 6g). The most prominent feature upon room-temperature exposure of 0.15 L water is the band at 2725 cm^{-1}, which is accompanied by less intense OD contributions at higher frequencies as well as broad signals at 2600 and 2350 cm^{-1}. According to the STM investigations, water/hydroxyl chains as well as smaller water aggregates are present on the surface under these conditions (Figure 6i,j).[30] Calculated anharmonic spectra for the $5D_2O/(3 \times 4)CaO(001)$ water structure attribute the 2725, 2600, and 2350 cm^{-1} bands to the free and surface OD groups of the tetramer units and to the coupled symmetric and antisymmetric stretch vibrations of surface OD in the linker units of the chains.[30] With increasing coverage, an OD signal at 2717 cm^{-1} appears, and the broad signal at 2600 cm^{-1} increases in intensity. Consistent with the STM observations (Figure 6k), this trend reflects the transition from the ordered, low-coverage phase to the disordered, high-coverage phase.[41]

OD groups with a frequency of 2717 cm^{-1} are characteristic of fully hydroxylated surfaces, as prepared by procedures 2 and 3 here. Presenting a structural model for hydroxyl groups appears to be difficult, as their surface arrangement is disordered according to STM. Nevertheless, recent findings from theoretical modeling provide some ideas on the possible nature of high-coverage hydroxyl units on the CaO surface. The reactive force field study by Manzano et al.[41] indicates a transition to a disordered, hydroxylated CaO surface when the water coverage approaches 1 ML, in agreement with our STM observations. In addition, their results show that solvated Ca^{2+} ions start to form at the surface at water coverages above 1 ML. Ončák et al. performed molecular dynamics simulations for 2 ML of water on MgO(001) and found several stable structures of solvated Mg^{2+} ions:[42] The contact ion pair, the solvent-separated ion pair, and the STRIPE model all feature hydroxyl groups linking solvated Mg^{2+} and surface Mg^{2+}.[42] We propose that, because of the same lattice type, the stabilization of similar solvated structures is also possible on CaO(001) and suggest that the 2717 cm^{-1} vibration can be attributed to OD groups of structures containing partially solvated Ca^{2+} ions. For the band at 2687 cm^{-1}, which appears only after extensive hydroxylation of CaO (procedure 3) involving subsurface hydroxylation, we follow Low et al.'s interpretation[22] and assign it to OD vibrations in $Ca(OD)_2$-like structures. The assignment of the main observed OD vibrations to specific water adsorption structures is summarized in Figure 7.

Finally, we comment on the thermal stability of the hydroxylated CaO surfaces. According to our XPS and IRAS results (Figure 4), two different water-loss processes above room temperature can be distinguished that depend on the

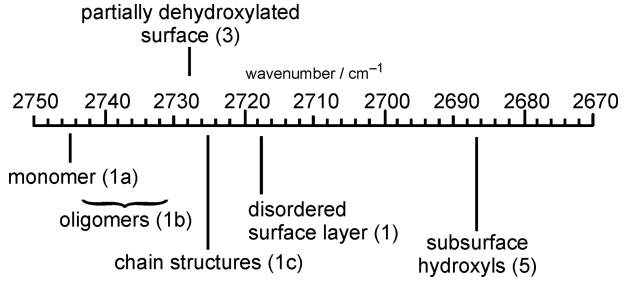

Figure 7. Summary and assignment of vibrations of OD groups on CaO near 2700 cm^{-1} according to the results of the present study.

DOI: 10.1021/acs.jpcc.6b00433
J. Phys. Chem. C 2016, 120, 5565−5576

hydroxylation pathway of CaO. After water exposure at room temperature at either low pressure (UHV, procedure 1) or elevated pressure (submillibar, procedure 3), dehydroxylation occurs between 400 and 600 K, being typical for water or air-exposed CaO.[16] The remaining OD groups exhibit a vibrational frequency of 2728 cm^{-1}, slightly different from those obtained at similar coverage during water adsorption (2725 cm^{-1}). The change reflects the different surface morphology of the partially dehydroxylated compared to that of the partially hydroxylated CaO surface. Although the surface structure remains more or less intact during hydroxylation up to a critical coverage, partial dehydroxylation from a fully hydroxylated surface necessarily creates a reconstructed surface with a changed binding environment, explaining the shifts in OD stretching frequencies. According to our observations, complete dehydroxylation and reordering of the CaO surface occurs only after annealing at 1000 K. For CaO hydroxylated by procedure 2 (UHV, 100 K), additional water loss occurs already between 300 and 400 K (Figure 4) when the water coverage drops from 1 to 0.6 ML, a value that is only slightly higher than that on the room-temperature-dosed sample (procedure 1) upon heating to 400 K. Despite this similarity in coverage, the corresponding IRA spectra are different. In particular, the dominance of the 2717 cm^{-1} band in spectrum 2 at 400 K (Figure 4c) suggests that samples exposed to water at low temperature exhibit a higher degree of structural disorder than those exposed at room temperature (for dosing under UHV conditions), which might be related to the larger sticking and longer contact time of water when condensed onto the surface at low temperature. The water loss between 300 and 400 K seen for procedure 2 might, therefore, be due to the desorption of structural water weakly bound to the disordered hydroxylated surface. We note that the results for our hydroxylation procedure 2 can be directly compared to the work of Iedema et al., who obtained a major water desorption signal at 360 K in temperature-programmed desorption,[26] in agreement with our observations.

3.4. Comparison of Experimental and Calculated O 1s Core-Level Spectra. To elucidate the contributions of different water/hydroxyl species to the experimental O 1s XP spectra, we present calculated core-level spectra for selected adsorption structures in Figure 8. [See the Supporting Information for the complete data set and the employed $12D_2O/(3 \times 4)CaO(001)$ and $Ca(OD)_2$ structure models.] The sticks represent the individual final-state core-level BEs of the various components (molecular water, green; surface OD, blue; free OD, red; surface O, gray; second-layer O, black), whereas the envelope was produced by Gaussian broadening (1 eV fwhm) to facilitate comparison with experiment.

We note that our calculated spectra for water on CaO(001) are in good agreement with similar calculations performed on MgO(001)[43] in terms of the relative positions of different O species. In particular, the coverage-dependent shift of core-level BEs for water/hydroxyl species is clearly visible and can be explained by the increasing effect of hydrogen bonding and water coordination. The smallest core-level shifts (CLSs) with respect to O in bulk CaO are found for OD_f (red), evolving from 1.26 eV ($1D_2O$) and 1.60 eV ($5D_2O$) to 2.28 eV for $12D_2O$ per unit cell. The shifts become larger for O_sD (blue: 1.66, 2.59/3.02, and 3.60 eV for $1D_2O$, $5D_2O$, and $12D_2O$, respectively) and are most pronounced for molecular water (green: 3.26 eV for $5D_2O$ and 3.95/4.71 eV for $12D_2O$). Apparently, a clear distinction of different water/hydroxyl species is hampered by the small BE separation of the

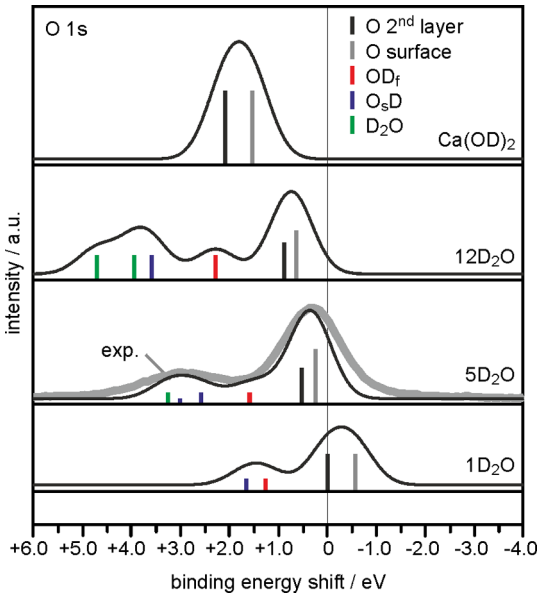

Figure 8. Calculated O 1s core-level binding energy shifts [referenced to the core-level binding energy of an O atom in the CaO bulk] for different water/CaO adsorption phases and $Ca(OD)_2$ (sticks). The colors of the sticks represent the various oxygen species (black and gray, second-layer O and surface O; red, OD_f; blue, O_sD; green, D_2O). To facilitate comparison with experimental spectra, the stick spectra have been broadened by Gaussians with 1 eV fwhm (black lines above the stick spectra). The experimental O 1s photoemission spectrum corresponding to hydroxylation procedure 1 is displayed for comparison (thick gray trace).

individual components, as well as by the relatively broad peaks in the experimental XP spectra. Only for adstructures with an excess of molecular or dissociated water (e.g., for $1D_2O$ with only dissociated water or for $12D_2O$ with 70% molecules) might the CLS and intensity differences be sufficient to separate the various components in the experiments. Conversely, a broad and featureless band necessarily appears for configurations with a comparable number of molecular and dissociated species (e.g., $5D_2O$ with three dissociated and two molecular species).

Despite this difficulty, the calculated core-level spectrum for the $5D_2O$ chain structure reproduces well the experimental results obtained for low water dosages according to procedure 1 (gray line in Figure 8). Together with the STM and IRAS data presented above, this can be taken as additional, yet weaker proof for the existence of the water/hydroxyl chains on the CaO(001) surface. We note, however, that, in general, the O 1s XP spectra of hydroxylated CaO films produced by procedures 1, 2, and 3 are rather similar, despite of the different oxide-to-water/hydroxyl peak intensity ratios (Figure 1a). Consequently, they can not be used to distinguish between the different adsorption structures on the CaO surface. This insensitivity might be explained with an increasing structural inhomogeneity of the water/CaO system, especially at high water dosages, when several ordered and disordered configurations, including a $Ca(OD)_2$ phase, coexist on the surface. This, in turn, results in strongly overlapping signal contributions and relatively broad spectra, as found in the experiments. Note that differentiation between molecular and dissociated water was possible for ordered monolayers on MgO(001), by comparing measured and calculated O 1s core-level BEs.[43,44]

DOI: 10.1021/acs.jpcc.6b00433
J. Phys. Chem. C 2016, 120, 5565−5576

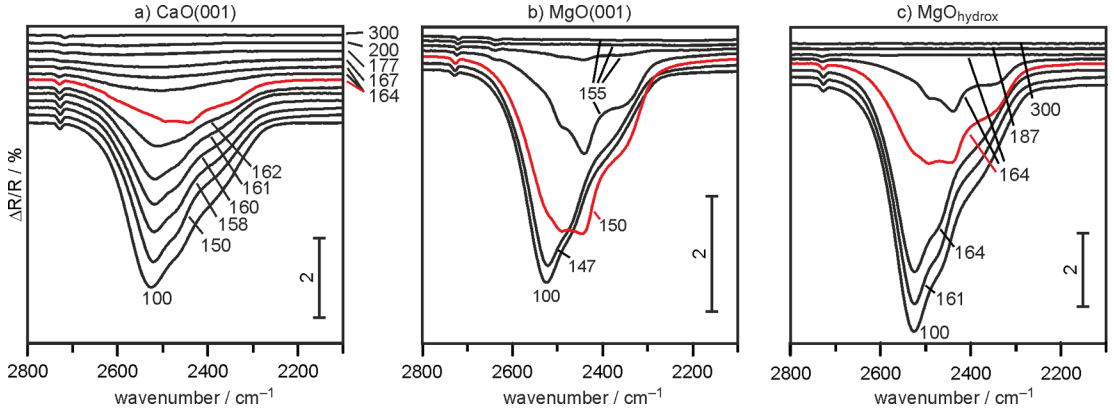

Figure 9. IRA spectra collected from (a) CaO(001) films, (b) 2-ML MgO(001)/Ag(001) films, and (c) hydroxylated 30-ML MgO films with a hydroxyl coverage of 0.7 ML, after exposure to 5 L of D_2O at 100 K and subsequent annealing to the indicated temperatures. At 100 K, amorphous solid water is formed on all sample surfaces. The characteristic change in the spectral profile with increasing temperature (indicated by the red spectra) corresponds to the transition to crystalline ice. Note that the transition temperatures are markedly different for hydroxylated (CaO and MgO_{hydr}) and nonhydroxylated [MgO(001)] surfaces.

3.5. Ice Desorption and the Phase Transition of Amorphous Solid Water (ASW) to Crystalline Ice (CI). Our XPS and IRAS analysis of water adsorption on CaO(001) (Figures 2c,d and 3c) revealed that water dissociates already at 100 K, which suggests that the CaO/ice interface consists of a hydroxyl layer. This gives rise to the question of the role of these interfacial hydroxyl groups in the structure of the ice layer, in particular, in the transition from amorphous solid water (ASW) to crystalline ice (CI). The influence of the wettability of interfaces on the ASW−CI transition and ice desorption was studied two decades ago, using mixed self-assembled monolayers consisting of alkanethiols with either $-CH_3$ or −OH termination on Au(111) as substrates.[45,46] That study revealed that both the transition and desorption temperature of ice depend strongly on the substrate functionality, showing clear inhibition of the ASW−CI transition and an increase of the ice desorption temperature on the more hydrophilic (−OH-terminated) interfaces. This effect was explained in terms of the stronger hydrogen-bond interaction between ice and the OH-terminated interface as compared to the hydrophobic (CH_3-terminated) interface. In the present study, a similar approach was used to alter the properties of ice at interfaces. However, instead of functionalizing the substrate with foreign molecules, we used the intrinsic reactivity of the oxide surface toward water as a tuning factor.

Figure 9a presents IRA spectra taken in the temperature range between 100 and 300 K of a water ice layer grown on clean CaO(001) at 100 K. The freshly grown ice layer (5-L dose at 100 K) exhibits typical absorption features of ASW, with a small band at 2730 cm^{-1} and a broad band in the hydrogen-bonded region below 2600 cm^{-1}. Heating to 162 K causes only a reduction of the absorption intensity but no change in the spectral profile, suggesting that the ice layers desorb from the amorphous state. At 164 K, when almost the complete layer has desorbed, the phase transition from ASW to CI occurs, as indicated by the appearance of a sharp band at 2440 cm^{-1} (red spectrum). This feature disappears during isothermal desorption at 164 K, and subsequently recorded IRA spectra show a featureless profile ascribed to disordered water/hydroxyl structures.

For comparison, the thermal behavior of ice on both hydroxyl-free and hydroxyl-covered MgO surfaces was investigated. For the former sample, a 2-ML MgO(001)/Ag(001) film was chosen, whereas a hydroxylated 30-ML MgO film, MgO_{hydr},[47] with θ(OD) ≈ 0.7 ML was employed in the latter case. The results obtained for the two systems are shown in panels b and c, respectively, of Figure 9. Comparing the IR data acquired from the MgO(001) and MgO_{hydr} surfaces underpins the discussion of the effect of interfacial hydroxyl groups, because water adsorption at low temperature on pristine MgO(001) leads to the formation of an ordered interfacial water monolayer, which is expected to weakly interact with ice layers.[44,48] At 100 K, ice layers on the pristine MgO(001) surface exhibit a typical ASW profile, and the ASW → CI transition occurs at ∼150 K, again as evidenced by the development of the IR signal at 2440 cm^{-1} (Figure 9b). This observation agrees well with the results obtained on thick MgO(001) films.[48] The ASW layers produced upon exposure of MgO_{hydr} to 5 L of D_2O at 100 K give rise to the same absorption features (Figure 9c). However, the ASW−CI transition is delayed on MgO_{hydr} as compared to that on bare MgO and is preceded by water desorption. In fact, the ASW layer on MgO_{hydr} partially desorbs as the temperature is increased to 164 K and transforms into CI only in the later stages of isothermal treatment at 164 K. The critical temperature for the phase transition is therefore about 10 K higher over MgO_{hydr} than over bare MgO surfaces but similar to that for the water/CaO(001) system (see Figure 9a). These differences lend strong support to the idea that the properties of the interfacial water/hydroxyl layer, particularly its ability to interact through hydrogen bonding with second-layer water molecules, affect the thermal behavior of supported ice layers. Our results are thus in line with previous studies of ice on self-assembled monolayers that related the inhibition of the ASW−CI transition to stronger interfacial interactions enabled by an intermolecular H-bonding network.[45,46]

4. CONCLUSIONS

The results of this study, in combination with previous experimental and theoretical findings, allow the hydroxylation of CaO(001) to be divided into several stages. In the first stage of adsorption, small water/hydroxyl clusters are formed that aggregate into water/hydroxyl chains at water coverages up to ∼0.3 ML. As the coverage is increased to saturation at room temperature under UHV conditions (∼0.5 ML), the CaO(001) surface transforms into a disordered state with partially solvated

DOI: 10.1021/acs.jpcc.6b00433
J. Phys. Chem. C 2016, 120, 5565−5576

Ca^{2+} ions. A hydroxyl coverage of close to 1 ML is stabilized upon condensation of water at 100 K followed by subsequent warming to room temperature. This state contains weakly bound water, which desorbs at ~350 K. Partial hydroxylation of the subsurface layers, involving the transformation of CaO into a $Ca(OH)_2$-like state, occurs during exposure at elevated water partial pressure (submillibar range). The facile hydroxylation of CaO(001) even at low temperature (100 K) was shown to have a pronounced influence on the properties of adsorbed ice. The amorphous ice state is stabilized by hydrogen-bond interactions between the interfacial hydroxyls and the ice layers, leading to a higher ice desorption temperature and a delayed transition into crystalline ice as compared to that on the nonhydroxylated MgO(001) surface.

By combining spectroscopic data with microscopic information and the results of DFT calculations, a correlation between the hydroxyl stretching frequencies of the OD_f groups observed by IR spectroscopy and the hydroxylated surface phases present at various water/hydroxyl coverages could be established. According to this correlation, the stretching frequency of OD_f decreases with increasing water coverage, that is, increasing hydrogen-bond interactions between the surface hydroxyl groups and water molecules. Because of the high reactivity of the CaO surface toward water dissociation, the coordination of surface Ca^{2+} ions in several defect structures (step edges and corners, vacancy defects) is expected to play only a minor role for the assignment of the observed hydroxyl IR frequencies. This is in contrast to findings for the stretching frequencies of hydroxyls adsorbed on the less reactive MgO(001) surface, which exhibit a strong dependence on both hydrogen-bond interactions and cation coordination.[39]

■ ASSOCIATED CONTENT

Supporting Information

The Supporting Information is available free of charge on the ACS Publications website at DOI: 10.1021/acs.jpcc.6b00433.

DFT-derived water adsorption structures on CaO(001); calculated anharmonic vibrational frequencies of surface hydroxyl and water species; and calculated O 1s and Ca 2p core-level binding energies of CaO(001), $Ca(OD)_2$, and various water adsorption structures on CaO(001) (PDF)

■ AUTHOR INFORMATION

Corresponding Author

*E-mail: martin.sterrer@uni-graz.at. Phone: +43 316 380 1620.

Present Address

[§]Department of Chemical Physics, CAS Key Laboratory of Urban Pollutant Conversion and Synergetic Innovation Center of Quantum Information and Quantum Physics, University of Science and Technology of China, Hefei, Anhui 230026, China.

Notes

The authors declare no competing financial interest.

■ ACKNOWLEDGMENTS

This work was supported by collaborative research center 1109 sponsored by Deutsche Forschungsgemeinschaft and the European Union through ERC Starting Grant Agreement 280070. Y.F. is grateful to Takata Co. Ltd. and DAAD for a fellowship (A/09/72968).

■ REFERENCES

(1) Hodgson, A.; Haq, S. Water Adsorption and the Wetting of Metal Surfaces. *Surf. Sci. Rep.* **2009**, *64*, 381−451.

(2) Carrasco, J.; Hodgson, A.; Michaelides, A. A Molecular Perspective of Water at Metal Interfaces. *Nat. Mater.* **2012**, *11*, 667−674.

(3) Henrich, V. E.; Cox, P. A. *The Surface Science of Metal Oxides*; Cambridge University Press: Cambridge, U.K., 1996.

(4) Henderson, M. A. The Interaction of Water with Solid Surfaces: Fundamental Aspects Revisited. *Surf. Sci. Rep.* **2002**, *46*, 1−308.

(5) Wichtendahl, R.; Rodriguez-Rodrigo, M.; Härtel, U.; Kuhlenbeck, H.; Freund, H.-J. Thermodesorption of CO and NO from Vacuum-Cleaved NiO(100) and MgO(100). *Phys. Stat. Sol. A* **1999**, *173*, 93−100.

(6) Barth, C.; Henry, C. R. Atomic Resolution Imaging of the (001) Surface of UHV Cleaved MgO by Dynamic Scanning Force Microscopy. *Phys. Rev. Lett.* **2003**, *91*, 196102.

(7) Ashworth, T. V.; Pang, C. L.; Wincott, P. L.; Vaughan, D. J.; Thornton, G. Imaging in Situ Cleaved MgO(100) with Non-Contact Atomic Force Microscopy. *Appl. Surf. Sci.* **2003**, *210*, 2−5.

(8) Wu, M.-C.; Corneille, J. S.; Estrada, C. A.; He, J.-W.; Goodman, D. W. Synthesis and Characterization of Ultra-Thin MgO Films on Mo(100). *Chem. Phys. Lett.* **1991**, *182*, 472−478.

(9) Wollschläger, J.; Erdös, D.; Schröder, K.-M. The Formation of Mosaics during the Reactive Growth of MgO Films on Ag(100). *Surf. Sci.* **1998**, *402−404*, 272−276.

(10) Marchese, L.; Coluccia, S.; Martra, G.; Zecchina, A. Dynamic and Static Interactions in CO Layers Adsorbed on MgO Smoke (100) Facelets: A FTIR and HRTEM study. *Surf. Sci.* **1992**, *269−270*, 135−140.

(11) Knözinger, E.; Diwald, O.; Sterrer, M. Chemical Vapour Deposition—A New Approach to Reactive Surface Defects of Uniform Geometry on High Surface Area Magnesium Oxide. *J. Mol. Catal. A: Chem.* **2000**, *162*, 83−95.

(12) Ho, C. S.; Shih, S. M. $Ca(OH)_2$/Fly Ash Sorbents for SO_2 Removal. *Ind. Eng. Chem. Res.* **1992**, *31*, 1130−1135.

(13) Hu, G. L.; Dam-Johansen, K.; Wedel, S.; Hansen, J. P. Review of the Direct Sulfation Reaction of Limestone. *Prog. Energy Combust. Sci.* **2006**, *32*, 386−407.

(14) Blamey, J.; Anthony, E. J.; Wang, J.; Fennell, P. S. The Calcium Looping Cycle for Large-Scale CO_2 Capture. *Prog. Energy Combust. Sci.* **2010**, *36*, 260−279.

(15) Lu, H.; Reddy, E. P.; Smirniotis, P. G. Calcium Oxide Based Sorbents for Capture of Carbon Dioxide at High Temperatures. *Ind. Eng. Chem. Res.* **2006**, *45*, 3944−3949.

(16) Granados, M. L.; Poves, M. D. Z.; Alonso, D. M.; Mariscal, R.; Galisteo, F. C.; Moreno-Tost, R.; Santamaria, J.; Fierro, J. L. G. Biodiesel from Sunflower Oil by using Activated Calcium Oxide. *Appl. Catal., B* **2007**, *73*, 317−326.

(17) Petitjean, H.; Chizallet, C.; Krafft, J. M.; Che, M.; Lauron-Pernot, H.; Costentin, G. Basic Reactivity of CaO: Investigating Active Sites under Operating Conditions. *Phys. Chem. Chem. Phys.* **2010**, *12*, 14740−14748.

(18) Albuquerque, M. C. G.; Jiménez-Urbistondo, I.; Santamaría-González, J.; Mérida-Robles, J. M.; Moreno-Tost, R.; Rodríguez-Castellón, E.; Jiménez-López, A.; Azevedo, D. C. S.; Cavalcante, C. L., Jr.; Maireles-Torres, P. CaO Supported on Mesoporous Silicas as Basic Catalysts for Transesterification Reactions. *Appl. Catal., A* **2008**, *334*, 35−43.

(19) Kouzu, M.; Kasuno, T.; Tajika, M.; Sugimoto, Y.; Yamanaka, S.; Hidaka, J. Calcium Oxide as a Solid Base Catalyst for Transesterification of Soybean Oil and its Application to Biodiesel Production. *Fuel* **2008**, *87*, 2798−2806.

(20) Sun, P.; Grace, J. R.; Lim, C. J.; Anthony, E. J. Investigation of Attempts to Improve Cyclic CO_2 Capture by Sorbent Hydration and Modification. *Ind. Eng. Chem. Res.* **2008**, *47*, 2024−2032.

(21) Yin, J. J.; Qin, C. L.; An, H.; Veeraragavan, A.; Feng, B. Influence of Hydration by Steam/Superheating on the CO_2 Capture Perform-

DOI: 10.1021/acs.jpcc.6b00433
J. Phys. Chem. C 2016, 120, 5565−5576

ance and Physical Properties of CaO-Based Particles. *Ind. Eng. Chem. Res.* **2013**, *52*, 18215−18224.
(22) Low, M. J. D.; Takezawa, N.; Goodsel, A. J. Infrared Study of Hydroxyls on Active CaO. *J. Colloid Interface Sci.* **1971**, *37*, 422−429.
(23) Fubini, B.; Bolis, V.; Bailes, M.; Stone, F. S. The Reactivity of Oxides with Water Vapor. *Solid State Ionics* **1989**, *32*−*33*, 258−272.
(24) Liu, P.; Kendelewicz, T.; Brown, G. E.; Parks, G. A.; Pianetta, P. Reaction of Water with Vacuum-Cleaved CaO(100) Surfaces: An X-ray Photoemission Spectroscopy Study. *Surf. Sci.* **1998**, *416*, 326−340.
(25) Bebensee, F.; Voigts, F.; Maus-Friedrichs, W. The Adsorption of Oxygen and Water on Ca and CaO Films Studied with MIES, UPS and XPS. *Surf. Sci.* **2008**, *602*, 1622−1630.
(26) Iedema, M. J.; Kizhakevariam, N.; Cowin, J. P. Mixed Oxide Surfaces: Ultrathin Films of $Ca_xMg_{(1-x)}O$. *J. Phys. Chem. B* **1998**, *102*, 693−700.
(27) Shao, X.; Myrach, P.; Nilius, N.; Freund, H. J. Growth and Morphology of Calcium Oxide Films Grown on Mo(001). *J. Phys. Chem. C* **2011**, *115*, 8784−8789.
(28) Shao, X.; Prada, S.; Giordano, L.; Pacchioni, G.; Nilius, N.; Freund, H. J. Tailoring the Shape of Metal Ad-Particles by Doping the Oxide Support. *Angew. Chem., Int. Ed.* **2011**, *50*, 11525−11527.
(29) Cui, Y.; Shao, X.; Baldofski, M.; Sauer, J.; Nilius, N.; Freund, H. J. Adsorption, Activation, and Dissociation of Oxygen on Doped Oxides. *Angew. Chem., Int. Ed.* **2013**, *52*, 11385−11387.
(30) Zhao, X. H.; Shao, X.; Fujimori, Y.; Bhattacharya, S.; Ghiringhelli, L. M.; Freund, H. J.; Sterrer, M.; Nilius, N.; Levchenko, S. V. Formation of Water Chains on CaO(001): What Drives the 1D Growth? *J. Phys. Chem. Lett.* **2015**, *6*, 1204−1208.
(31) Blum, V.; Gehrke, R.; Hanke, F.; Havu, P.; Havu, V.; Ren, X. G.; Reuter, K.; Scheffler, M. Ab initio Molecular Simulations with Numeric Atom-Centered Orbitals. *Comput. Phys. Commun.* **2009**, *180*, 2175−2196.
(32) Perdew, J. P.; Burke, K.; Ernzerhof, M. Generalized Gradient Approximation made Simple. *Phys. Rev. Lett.* **1996**, *77*, 3865−3868.
(33) Heyd, J.; Scuseria, G. E.; Ernzerhof, M. Hybrid Functionals Based on a Screened Coulomb Potential. *J. Chem. Phys.* **2003**, *118*, 8207−8215.
(34) Heyd, J.; Scuseria, G. E.; Ernzerhof, M. Erratum: "Hybrid Functionals Based on a Screened Coulomb Potential" [*J. Chem. Phys.* 118, 8207 (2003)]. *J. Chem. Phys.* **2006**, *124*, 219906.
(35) Wilson, E. B., Jr.; Decius, J. C.; Cross, P. C. *Molecular Vibrations: The Theory of Infrared and Raman Vibrational Spectra*; Courier Corporation: North Chelmsford, MA, 2012.
(36) Janak, J. F. Proof that $\partial E/\partial n_i = \varepsilon$ in Density-Functional Theory. *Phys. Rev. B: Condens. Matter Mater. Phys.* **1978**, *18*, 7165−7168.
(37) Lizzit, S.; Baraldi, A.; Groso, A.; Reuter, K.; Ganduglia-Pirovano, M. V.; Stampfl, C.; Scheffler, M.; Stichler, M.; Keller, C.; Wurth, W.; Menzel, D. Surface Core-Level Shifts of Clean and Oxygen-Covered Ru(0001). *Phys. Rev. B: Condens. Matter Mater. Phys.* **2001**, *63*, 205419.
(38) Carrasco, J.; Illas, F.; Lopez, N. Dynamic Ion Pairs in the Adsorption of Isolated Water Molecules on Alkaline-Earth Oxide (001) Surfaces. *Phys. Rev. Lett.* **2008**, *100*, 016101.
(39) Chizallet, C.; Costentin, G.; Che, M.; Delbecq, F.; Sautet, P. Infrared Characterization of Hydroxyl Groups on MgO: A Periodic and Cluster Density Functional Theory Study. *J. Am. Chem. Soc.* **2007**, *129*, 6442−6452.
(40) Lutz, H. D.; Möller, H.; Schmidt, M. Lattice vibration spectra. Part LXXXII. Brucite-Type Hydroxides $M(OH)_2$ (M = Ca, Mn, Co, Fe, Cd)—IR and Raman Spectra, Neutron Diffraction of $Fe(OH)_2$. *J. Mol. Struct.* **1994**, *328*, 121−132.
(41) Manzano, H.; Pellenq, R. J. M.; Ulm, F. J.; Buehler, M. J.; van Duin, A. C. T. Hydration of Calcium Oxide Surface Predicted by Reactive Force Field Molecular Dynamics. *Langmuir* **2012**, *28*, 4187−4197.
(42) Ončák, M.; Włodarczyk, R.; Sauer, J. Water on the MgO(001) Surface: Surface Reconstruction and Ion Solvation. *J. Phys. Chem. Lett.* **2015**, *6*, 2310−2314.
(43) Paz-Borbón, L. O.; Hellman, A.; Grönbeck, H. Simulated Photoemission Spectra of Hydroxylated MgO(100) at Elevated Temperatures. *J. Phys. Chem. C* **2012**, *116*, 3545−3551.
(44) Wlodarczyk, R.; Sierka, M.; Kwapien, K.; Sauer, J.; Carrasco, E.; Aumer, A.; Gomes, J. F.; Sterrer, M.; Freund, H. J. Structures of the Ordered Water Monolayer on MgO(001). *J. Phys. Chem. C* **2011**, *115*, 6764−6774.
(45) Engquist, I.; Lundström, I.; Liedberg, B. Temperature-Programmed Desorption and Infrared Studies of D_2O Ice on Self-Assembled Alkanethiolate Monolayers: Influence of Substrate Wettability. *J. Phys. Chem.* **1995**, *99*, 12257−12267.
(46) Engquist, I.; Lundström, I.; Liedberg, B.; Parikh, A. N.; Allara, D. L. Infrared Characterization of Amorphous and Polycrystalline D_2O Ice on Controlled Wettability Self-Assembled Alkanethiolate Monolayers. *J. Chem. Phys.* **1997**, *106*, 3038−3048.
(47) Carrasco, E.; Brown, M. A.; Sterrer, M.; Freund, H. J.; Kwapien, K.; Sierka, M.; Sauer, J. Thickness-Dependent Hydroxylation of MgO(001) Thin Films. *J. Phys. Chem. C* **2010**, *114*, 18207−18214.
(48) Carrasco, E.; Aumer, A.; Gomes, J. F.; Fujimori, Y.; Sterrer, M. Vibrational Spectroscopic Observation of Ice Dewetting on MgO(001). *Chem. Commun.* **2013**, *49*, 4355−4357.

DOI: 10.1021/acs.jpcc.6b00433
J. Phys. Chem. C 2016, 120, 5565−5576